Design of a microbial contamination detector and analysis of error sources in its optical path

Chao Zhang, Xiang Yu*, Xingju Liu and Lei Zhang
School of Engineering and Technology, China University of Geosciences (Beijing), Beijing, China

Abstract: Microbial contamination is a growing concern in the food safety today. To effectively control the types and degree of microbial contamination during food production, this paper introduces a design for a microbial contamination detector that can be used for quick in-situ examination. The designed detector can identify the category of microbial contamination by locating its characteristic absorption peak and then can calculate the concentration of the microbial contamination by fitting the absorbance vs. concentration lines of standard samples with gradient concentrations. Based on traditional scanning grating detection system, this design improves the light splitting unit to expand the scanning range and enhance the accuracy of output wavelength. The motor rotation angle φ is designed to have a linear relationship with the output wavelength angle λ, which simplifies the conversion of output spectral curves into wavelength vs. light intensity curves. In this study, we also derive the relationship between the device's major sources of errors and cumulative error of the output wavelengths, and suggest a simple correction for these errors. The proposed design was applied to test pigments and volatile basic nitrogen (VBN) which evaluated microbial contamination degrees of meats, and the deviations between the measured values and the pre-set values were only in a low range of 1.15% - 1.27%.

Keywords: Microbial contamination detection, spectrophotometric method, Light splitting unit, wavelength error analysis.

INTRODUCTION

It is well known that microbial contamination may happen during food products. However, microbial contamination is known to be toxic at different levels and may cause deformity or cancer. For current detection methods, contaminations need to be separated from the food samples in order to be detected. These methods include high performance liquid chromatography (HPLC) (Zakharova *et al*., 2013) and thin layer chromatography (TLC) (Baranowska *et al*., 2004), which are procedurally complicated and time-consuming. To cope with growing food safety concerns in developing countries, where food production is very much decentralized, a device that is able to rapidly detect microbial contamination is highly desirable. Such a device should be capable of detecting a wide range of microbial contamination with high precision while also being easy to operate and maintain.

The spectrophotometric method is simple and fast substances in detecting substances, thus is suitable for rapid detection of microbial contamination. Currently spectrophotometry has been successfully used to analyze Cr (III) and Cr (VI) in water samples (Vargas-Vasquez *et al*., 2010). There are two major types of standard optical system used for spectrophotometers: fixed gratings and scanning gratings (Schmidt, 1995). The fixed gratings usually use an array type photo detector, such as a photo diode array (PDA) or a charge coupled device (CCD) (Prevatt, 2004), which is capable of multi-channel simultaneous exposures and rapid detection. However, restrictions in the length of the array detector and the number of pixels make it difficult for the resolution to be higher than 0.1 nm, unless the spectral range is narrow. Meanwhile, because of the lack of an exit slit, there are deficiencies in the system's ability to suppress stray light (Zonios, 2010). Scanning grating detection systems, on the other hand, are high resolutions and can suppress stray light by adjustment of the exit and entrance slits. However, the small scanning range is a notable, drawback, which limits the range of microbial contaminations that can be detected. In this study, we attempted to improve the scanning grating system by (i) expanding the scanning range by improving the spectral structure, (ii) enhancing the spectral accuracy by reducing the linear coefficient between the output wavelength and the dislocation of the motor angle, and (iii) proposing a simple and effective modification method by analyzing the cumulative error in the output wavelength caused by the major sources of error in the scanning process. This proposed system is expected to have a wide scanning range and high detection precision, to be easy to modify, and to be suitable for *rapid in-situ* detection.

MATERIAL AND METHODS

Detection principle and design ideas

When parallel monochromatic light with intensity I_0 travels through a uniform non-scattering liquid, the quantitative relationship between the degree of light absorption of the solution, the optical path, and the

*Corresponding author: e-mail: yuxiang690625@aliyun.com

solution concentration is consistent with the Lambert - Beer law, namely,

$$A = -\log\frac{I}{I_0} = KbC, \quad (1)$$

Where A is the absorbance of the solution, I is the intensity of the light travelling through the solution, I_0 is the intensity of light travelling through air, K is the molar absorption coefficient, b is the optical path, and C is the solution concentration. It can be seen that when a beam of light travels through the solution containing the light-absorbing substance, if the optical path and the molar absorption coefficient are constant, the absorbance A of the solution is proportional to the concentration of the component of the solution to be measured (Langhals *et al.*, 2000).

Gratings are commonly used for chromatic dispersion. The typical structure of a grating is illustrated in fig. 1(a), where a glass blank (4) has an aluminum coating (3), and on the aluminum coating are dense parallel grooves. Diffraction occurs when composite parallel light (1) hits the surface of the aluminum grooves (Rajan *et al.,* 2012). As shown in fig. 1 (b), parallel light hits the grating with an incident angle a, and the diffraction light in the exit direction b is overlapped. When the incident direction a and the exit direction b are fixed and on the same side of the grating normal, the difference between the optical paths of two adjacent grooves in the exit direction is $OG + OM$, shown in fig. 1(b), and the phase difference of the light with wavelength λ is

$$\frac{2\pi(OG+OM)}{\lambda} = \frac{2\pi c(\sin a + \sin b)}{\lambda}, \quad (2)$$

Where c is the grating constant, and the maximum value of the intensity of the light with wavelength λ in the exit direction is obtained when the phase difference is $2k\pi$. The grating equation for the case where the incident direction a and the exit direction b are on the same side of the grating normal n is thus obtained:

$$c(\sin b + \sin a) = k\lambda. \quad (3)$$

Similarly, when the incident direction a and the exit direction b are on opposite sides of the grating normal n, the optical path difference of the two adjacent grooves in the exit direction is $OM - OG$, and the grating equation is thus (Lu *et al.,* 2012):

$$c(\sin b - \sin a) = k\lambda. \quad (4)$$

Since the precision of fixed gratings is limited by their ability to suppress stray light, we opted to implement our design using a scanning grating, focusing on expanding its scanning range, improving its light splitting precision, and equipping it with easy-correction capabilities as a requirement for on-site usage. To achieve these purposes and test the detection accuracy of this system, we concentrated our efforts in the following areas. (i) The design for optical path for detection. This component decomposes the composite light emitted from the light source using the grating, and outputs monochromatic light for detection. The photoelectric conversion was achieved by a silicon photocell after the monochromatic light transmits the sample to be examined; (ii) The design of the light splitting unit. This component outputs monochromatic light of different wavelengths by rotating the grating to accomplish the spectral line scanning. The equation describing the relationship between the output wavelength and the rotation angle of the stepper motor is derived from kinematic analysis, and indicates that the mechanism's output wavelength is proportional to the motor rotation angle and characterized by a wide scanning range. From this equation, the dependence on the primary mechanical errors and the cumulative error of the output wavelength is also evaluated, and an easy-correction method is proposed to offset the accumulated error; (iii) Testing actual pigments and at predetermined concentrations to measure the detection accuracy of this system. We tested the absorbance of sunset yellow and lemon yellow standard solutions whose concentrations are distributed on a gradient; fitted their absorbance vs. concentration lines; tested the absorbance of the sunset yellow and lemon yellow solutions, the concentrations of which were known; calculated the concentration using an interpolation method; and compared the measured value to the true value to test the system accuracy; (iv) Testing VBN with the standard solutions to test the capacity of this system for evaluation microbial contamination degrees of meats.

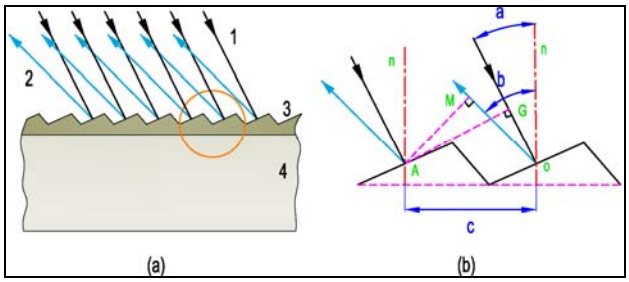

Fig. 1: Grating diagram: (a) grating structure diagram and (b) grating diffraction diagram

Design of the optical path

To produce monochromatic light output and achieve the required spectral scanning, the optical paths were designed as illustrated in fig. 2. After the composite light from source (1) is focused by the focusing lens (2), it hits the collimator lens (4) through slit (3) and forms parallel light. After dispersion by the grating (5), the parallel light rays of different wavelengths focus at different diffraction angles on the collecting mirror (6), which converges the parallel light rays onto different positions on the focusing surface. Finally, the monochromatic light is output from the exit slit (7) onto the focusing surface. The position of the exit slit (7) is fixed, and thus the incident direction and exit direction of the grating are fixed. When the stepper motor drives the grating to rotate, the wavelength of the exit light varies, thus achieving spectral scanning.

Monochromatic light rays of different wavelengths hit the silicon photovoltaic cell through cuvette containing the substance to be examined, and the silicon photocell converts this light intensity signal to an electrical signal output.

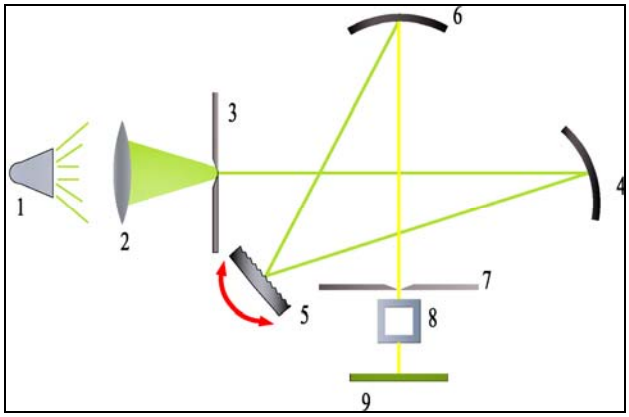

Fig. 2: Optical path design of the system (1) Light source, (2) focus lens, (3) entrance slit, (4) collimating lens, (5) grating, (6) collecting mirror, (7) exit slit, (8) cuvette, and (9) silicon photocell

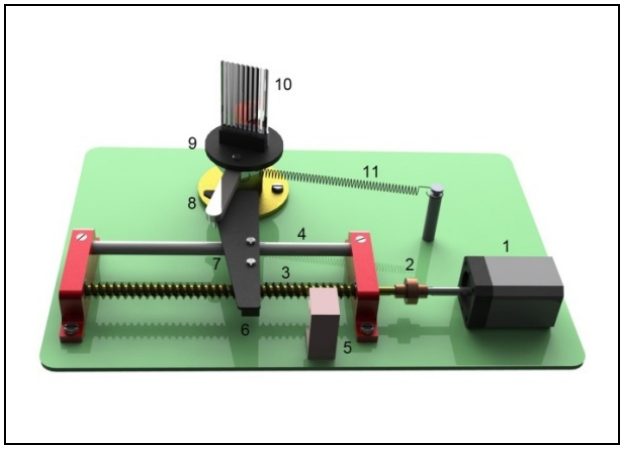

Fig. 3: Light splitting unit (1) Stepper motor, (2) coupling, (3) guide screw, (4) guide rod, (5) photoelectric switch, (6) slider with nut, (7) paddle, (8) sine bar, (9) grating tray, (10) grating, (11) spring

The core of the optical detection system is the light splitting unit that outputs different wavelengths of monochromatic light by rotating the grating. This unit determines the accuracy of the exit monochromatic light and the degree of difficulty in converting the output spectrum into wavelength-light intensity spectra that are physically meaningful. The light splitting unit is shown in fig. 3. The stepper motor (1) is connected to the guide screw (3) by the coupling (2); the slider with nut (6) and the paddle (7) are held together by screws; the screws clamp and hold the reflection grating (10) onto the grating tray (9); and the sine bar (8) and the grating tray (9) are also held together by screws. When the stepper motor rotates, the slider with nut (6) and the paddle (7) move back and forth under the direction of guide rod (4), thus propelling the sine bar (8) and driving the grating to rotate. The photoelectric switch (5) is used to determine the initial position of the paddle (7), i.e., the grating's initial angle ε. The accumulated error in the wavelength can be eliminated each time by resetting the photoelectric switch (5) on the scanning unit. The spring (11) presses the paddle (7) and the sine bar (8) together tightly to ensure precision in the movement and to provide the necessary moment needed for the grating's return trip.

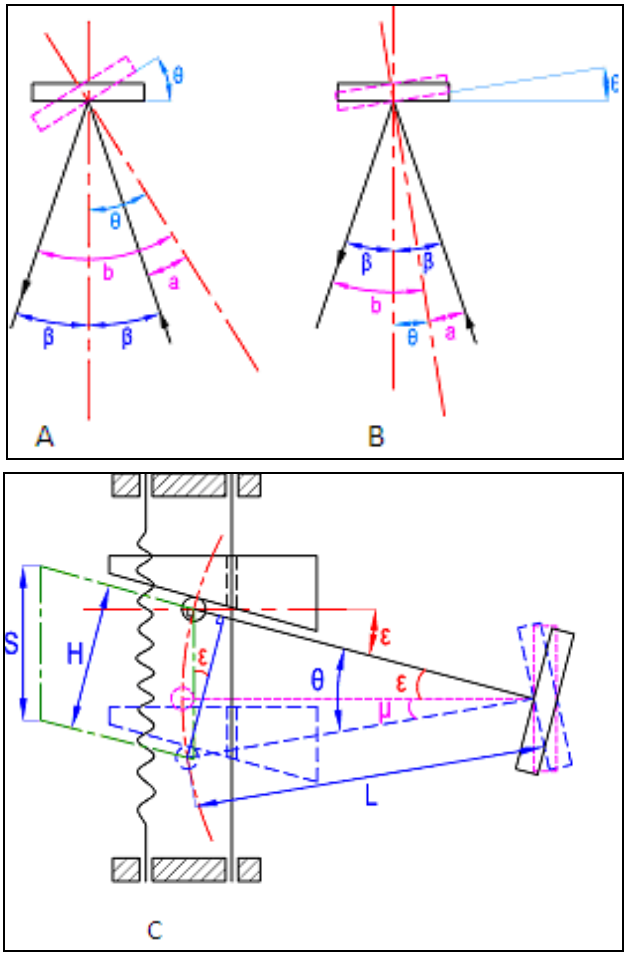

Fig. 4: Diagram of the movement of the light splitting unit for (a) a large rotation angle and (b) a small rotation angle; (c) diagram of light splitting unit.

RESULTS

Kinematic analysis of the light splitting unit

As shown in fig. 4, as the incident direction to and exit direction from the grating are fixed, when the grating spins, the incident angle a and the diffraction angle b of the exit direction shift, thus altering the wavelength of the light in the exit direction. β is the bisector of the angle formed by the incident direction and the exit direction of the grating at the initial position. When the grating angle θ is large, the incident direction and the exit direction are on

the same side of the grating normal after the rotation. As illustrated in fig. 4 (a), the angle formed by the incident direction and the grating normal after rotation is $a=\theta - \beta$, and the angle between the exit direction and the grating normal after rotation is $b=\theta + \beta$. Substituting these into the grating Eq. 3 for the case where the incident direction and the exit direction are on the same side of the grating normal n, using the sum and difference formulae, the following is obtained:

$$c(2\sin\theta\cos\beta) = k\lambda, \tag{5}$$

When the grating rotation angle θ is small, as shown fig. 4(b), and the incident direction and the exit direction are on opposite sides of the rotated grating normal, the angle between the incident direction and rotated grating normal is $a = \beta - \theta$, and the angle between the exit direction and the grating normal after rotation is $b = \theta + \beta$. When these are substituted into the grating Eq. 4, it can be simplified as

$$c(2\sin\theta\cos\beta) = k\lambda. \tag{6}$$

A comparison between Eq. 5 and Eq. 6 shows that both cases yield the same simplified results.

As indicated in fig. 4(c), when the paddle (7) pushes the sine bar (8) forward by a distance S, the rotation angle of the grating relative to the initial position is θ, and the angular dislocation of the stepper motor is φ. As the length of the sine bar is L, and the initial position angle of the unit is ε, then:

$$\sin\theta = \frac{H}{L} = \frac{S\cos\varepsilon}{L}. \tag{7}$$

Let the ball screw be h, then:

$$S = \frac{h\varphi}{2\pi}. \tag{8}$$

Once Eq. 7 and Eq. 8 are substituted into Eq. 5, the following is obtained:

$$\lambda = W \bullet \cos\varepsilon \bullet \varphi \ , \ \mathrm{W} = \frac{hc\cos\beta}{\pi kL}, \tag{9}$$

Where both W and $cos\varepsilon$ are constants, and therefore the stepper motor rotation angle φ and the wavelength λ in the exit direction have a linear relationship, which facilitates the conversion of the output spectral curves into wavelength vs. light intensity spectral curves. Compared to conventional spectral mechanisms, Eq. 9 has an extra $cos\varepsilon$ that can reduce the linear coefficient of the motor rotation angle φ and the selected wavelength λ in the exit direction, and thus improve the precision of the output wavelength. fig. 4 (c) indicates that when the space of the light splitting unit is the same, the grating's rotation angle of our design is $\theta = \varepsilon + \mu$, where ε is the initial angle of the unit, and μ is the rotation angle that is allowed for the grating in a traditional sinusoidal unit. It can be seen that the rotation range is now significantly expanded.

DISCUSSION

Errors in the light splitting unit: analysis and correction

Eq. 9 shows that the output wavelength error generated by the light splitting unit is primarily caused by the sine bar length error dL, the ball screw error dh, the grating constant error dc, and the initial position angle dislocation $\Delta\theta$. Once the unit has been fabricated, the above errors are all constants. This section focuses on the analyses of the impacts of the various errors on the wavelength output by the unit. The parameters used in this section are as follows: the output wavelength of the unit at the initial position, denoted by λ_0; the output wavelength at the terminal position, denoted as λ_1; when a certain range is scanned, the initial angular dislocation of the motor corresponding to λ_0 is recorded as φ_0, and the terminal angular dislocation corresponding to λ_1 is recorded as φ_1; and the motor rotation angle in the scanning range from λ_0 to λ_1, denoted as $\Delta\varphi$, $\Delta\varphi = \varphi_1 - \varphi_0$.

The impact of the sine bar length error dL on the output wavelength

The partial derivative of L is calculated from Eq. 9:

$$\begin{aligned} d\lambda &= -\frac{hc\cos\beta}{\pi kL^2} \bullet \cos\varepsilon \bullet \varphi \bullet dL \\ &= -W \bullet \cos\varepsilon \bullet \frac{dL}{L} \bullet \varphi. \end{aligned} \tag{10}$$

Then the accumulated error $\Delta\lambda$ of the unit when scanning from λ_0 to λ_1 is

$$\Delta\lambda = -W \bullet \cos\varepsilon \bullet \frac{dL}{L} \bullet \Delta\varphi. \tag{11}$$

Eq. 11 shows that the cumulative error $\Delta\lambda$ over the scanning interval has a linear relationship with the rotation angle of the stepper motor in that interval, i.e., when the initial angular dislocation of the motor is constant, a linear relationship exists between the accumulated error and the stepper motor's angular dislocation at the terminal position of the scanning interval.

The impact of the grating constant error dc on the output wavelength

The partial derivative of c is obtained from Eq. 9:

$$\begin{aligned} d\lambda &= \frac{h\cos\beta}{\pi kL} \bullet \cos\varepsilon \bullet \varphi \bullet dc \\ &= W \bullet \cos\varepsilon \bullet \frac{dc}{c} \bullet \varphi. \end{aligned} \tag{12}$$

Then the cumulative error $\Delta\lambda$ of the wavelength within the unit's scanning range is

$$\Delta\lambda = W \bullet \cos\varepsilon \bullet \frac{dc}{c} \bullet \Delta\varphi. \tag{13}$$

Eq. 13 indicates that the cumulative wavelength error $\Delta\lambda$ within the scanning interval that arises as a result of the grating constant dc has a linear relationship with the angle covered by the stepper motor within that scanning interval.

Effect of the guide screw error dh on the output wavelength

The partial derivative of h is obtained from Eq. 9:

$$d\lambda = \frac{c \bullet \cos\beta}{\pi k L} \bullet \cos\varepsilon \bullet \varphi \bullet dh = W \bullet \cos\varepsilon \bullet \frac{dh}{h} \bullet \varphi. \quad (14)$$

Then the cumulative error $\Delta\lambda$ of the wavelength within the scanning range of the unit is

$$\Delta\lambda = W \bullet \cos\varepsilon \bullet \frac{dh}{h} \bullet \Delta\varphi. \quad (15)$$

Equation 15 shows that the cumulative wavelength error Δλ within the scanning interval caused by the guide screw error dh has the same linear relationship with the rotation angle covered by the stepper motor in that scanning interval.

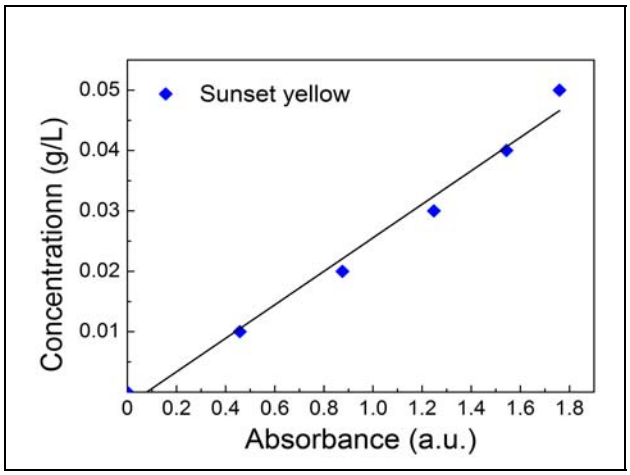

A

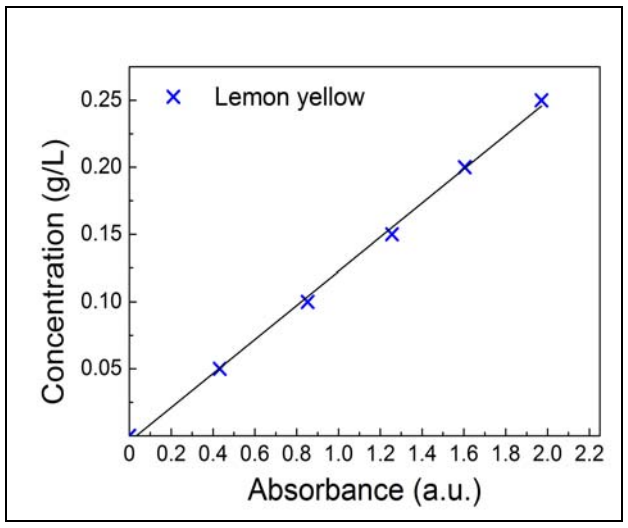

B

Fig. 5: Absorbance and concentration fits for sunset yellow and lemon yellow

Effect of the initial position angle dislocation Δθ on the output wavelength

For Eq. 5 to be valid, the central line of the sine bar at the initial position and the inclined plane of the slider bar are parallel. Let a clockwise dislocation occur to the sine bar in fig. 4(c), taken as the positive direction; then, the central line of the sine bar at the initial position forms an angle $\Delta\theta$ with the inclined plane of the slider bar, and Eq. 5 therefore becomes

$$k\lambda = 2c \bullet \cos\beta \sin(\theta + \Delta\theta) \quad (16)$$

$$\frac{k\lambda}{2c\cos\beta} = \sin\theta \bullet \cos\Delta\theta + \cos\theta \bullet \sin\Delta\theta. \quad (17)$$

Under normal circumstances, $\Delta\theta$ is very small, so an approximation can be made, such that

$$\frac{k\lambda}{2c\cos\beta} = \sin\theta + \cos\theta \bullet \Delta\theta = \frac{H}{L} + \sqrt{1-(\frac{H}{L})^2} \bullet \Delta\theta = \frac{H}{L} + \left[1 - \frac{H^2}{2L^2} + \frac{H^4}{8L^4} + \cdots\right] \bullet \Delta\theta. \quad (18)$$

Since the values of the items after $H^4/8L^4$ are so small, these items can be ignored. Substituting H = Scosε and Eq. 8 into Eq. 18, we can simplify the equation as follows:

$$\lambda = W\cos\varepsilon \bullet \varphi + \Delta\theta \bullet \frac{2c\cos\beta}{k} - \frac{h^2 c \bullet \cos^2\varepsilon \bullet \cos\beta \bullet \Delta\theta}{(2\pi L)^2 \bullet k} \bullet \varphi^2. \quad (19)$$

The output wavelength λ_0 at the initial position of the unit is subtracted from the terminal wavelength λ1 within the scanning interval:

$$\lambda_1 - \lambda_0 = W\cos\varepsilon \bullet \Delta\varphi - \frac{kW^2\cos^2\varepsilon \bullet \Delta\theta}{4c\cos\beta} \bullet (\varphi_1^2 - \varphi_0^2). \quad (20)$$

Since $\lambda_1 - \lambda_0$ is the true value within the scanning interval, and $W\cos\varepsilon \bullet \Delta\varphi$ is the value of the scanning displayed by the unit, then the error $\Delta\lambda$ within the scanning interval is

$$\Delta\lambda = \lambda_{display} - \lambda_{true} = W\cos\varepsilon \bullet \Delta\varphi - (\lambda_1 - \lambda_0) = \frac{kW^2\cos^2\varepsilon \bullet \Delta\theta}{4c\cos\beta} \bullet (\varphi_1^2 - \varphi_0^2). \quad (21)$$

Equation 21 shows that the angular dislocation of the stepper motor corresponding to the initial position is constant, and the accumulated error $\Delta\lambda$ within the scanning interval caused by the angle dislocation error $\Delta\theta$ at the initial position forms a quadratic relationship with the angular dislocation of the motor corresponding to the terminal position of the interval. Therefore, when the angular dislocation of the motor corresponding to the wavelength-scanning interval is very distant from the initial point, the growth rate of the error will be significantly faster.

The above analysis indicates that within the scanned interval, the relationship between the motor's rotation angle and the output wavelength error, which is caused collectively by the sine bar error, the grating constant error, and the guide screw error, is linear. Such an error can be completely eliminated by modifying the length of the sine bar. The error interval $\Delta\lambda$ caused by the angle dislocation $\Delta\theta$ at the initial position forms a quadratic relationship with the stepper motor angular dislocation at the terminal point of the scanning interval. This error can only be partially eliminated by modifying the sine bar length, and therefore when assembling the device, it must be ensured that the central line of the sine bar at the initial position is parallel to the slope of the slider bar.

Detection of pigments and volatile basic nitrogen

The proposed device is tested for real detection scenarios. The electronic state of each molecule contains rotation-vibration energy levels; when a molecule is irradiated, the vibrational and rotational energy level of the molecules transits from the ground state to the activated state. Different molecules require different amounts of energy to complete the energy transition. In other words, different wavelength photons are absorbed by different molecules and thus produce different characteristics, which are presented in their spectra. Pigments contained in a solution can thus be identified by locating their absorbance peaks. For example, the maximum absorption peaks for sunset yellow and lemon yellow are at 482 nm and 428 nm, respectively. It is known from Eq. 1 that the absorbance of the solution has a linear relationship with its concentration. This relationship between the absorbance and the concentration can be obtained from linear least squares fitting, and the solution concentration can be calculated by substituting the measured absorbance into the fitting line. The absorbance and concentration of standard solutions with sunset yellow and lemon yellow concentration gradients were fitted, and the results are presented in fig. 5.

The fitted line for sunset yellow that was obtained is $y= 0.02773x - 0.00219$, with a linear correlation coefficient of 99.2%, while the fitted line for lemon yellow is $y= 0.12682x - 0.00427$, with a linear correlation coefficient of 99.8%, indicating that the system is highly linear. The system performance verification indicates that the absorbance of the prepared 0.045g/L sunset yellow and lemon yellow standard solutions was 1.7037 and 0.3840, respectively. By determining the line fit, their concentrations were calculated to be 0.0450536g/L and 0.0444288g/L, respectively, and the errors were 1.19% and 1.27% relative to the true value, indicating that the system has high detection accuracy.

Meanwhile, this detector can be employed to in-situ detect microbial contaminations in foods. A typical example is VBN in meat products. The meats will spoil and produce ammonia and VBN under action of bacteria and enzymes, and VBN concentration can often be used to evaluate microbial contamination degrees of meats since VBN can induce the food poisoning. We used net pig hind legs meat in fresh as sample. Prepared the reagent for colorimetry: (i) uniformly mixed 1.5 ml solution of formal dehyde (360g/L) with 7.8 ml acetylacetone and (ii) diluted to 100 ml by buffer solution of sodium acetate- acetic acid with pH 5.61. Stored the sample at 7^{o}C in a thermostat, the VBN exhibited the color reaction and whose color turned into faint yellow, its maximum absorption peaks was at 412 nm. The detection result showed that the VBN concentration had a linear increase with storage day. As for the sample of 11 mg/100g, its VBN increased to 26 mg/100g at 8th storage day. Comparing with the standard solutions with known concentrations allowed us to see that the RSD (relative standard deviation) was 1.15%.

CONCLUSION

In order to effectively monitor the type and degree of microbial contamination in a timely manner, we proposed a design for a microbial contamination detection device. By improving the light splitting unit, we were able to amplify its detection range, improve its accuracy, and simplify its operations. We also derived the relationship between the output wavelength of the unit and the stepper motor angular dislocation and find that: (i) the stepper motor angular dislocation φ has a linear relationship with the selected wavelength λ in the exit direction, which can be used to facilitate system calibration and (ii) the introduction of cosε, in which ε is the initial position angle, reduces the linear coefficient of the motor rotation angle φ and the output wavelength λ, which improves the accuracy of the wavelength of the output monochromatic light. When the space of the light splitting unit is the same, the grating angle of our design is $\theta = \varepsilon + \mu$, i.e., the sum of the unit's initial rotation angle ε and the angular dislocation μ of conventional sine light splitting unit. Therefore, our design expands the range of the output wavelength of the monochromatic light, and thus allows the device to detect a wide range of microbial contamination.

The analysis of the error in the output wavelength showed that the errors caused by the sine bar error, grating constant error, and guide screw error are linearly related with the motor rotation angle within the scanning interval, and can be completely eliminated by modifying the length of the sine bar. The cumulative error $\Delta\lambda$ within the scanned interval caused by the angle dislocation $\Delta\theta$ at the initial position has a quadratic relationship with the terminal angular dislocation of the stepper motor within the scanning interval, and can only be partially eliminated by modifying the length of the sine bar. As a result, we must ensure that at the initial position the central line of the sine bar is parallel to the slide slope. The device was tested for real pigments. Fitting the absorbance vs.

concentration lines of standard sunset yellow and lemon yellow solutions with a concentration gradient, the linear correlation coefficient reached 99%. For the concentration detection test, we used two pigments and VBN solutions with a predetermined concentration of standard solutions, the deviations between the measured values and the pre-set values were only in a low range of 1.15 % - 1.27 %.

ACKNOWLEDGMENT

This work was supported by (i) the Natural Science Foundation of China under Grant 51071143; (ii) the Fundamental Research Funds for the Central Universities under Grant 2011YXL019 and 2010ZY40; and (iii) a Foundation for the Author of National Excellent Doctoral Dissertation of PR China under Grant FANEDD 201166.

REFERENCES

Baranowska I, Zydron M and Szczepanik K (2004). TLC in the analysis of food additives. *Jpc-j. Planar. Chromat.,* **17**(1): 54-57.

Langhals H, Abbt-Braun G and Frimmel FH (2000). Association of humic substances: Verification of Lambert-Beer law. *Acta. Hydroch. Hydrob.,* **28**(6): 329-332.

Lu W and Lu YY (2012). High order integral equation method for diffraction gratings. *J. Opt. Soc. Am. A-Opt. Image Sci. Vis.,* **29**(5): 734-740.

Prevatt J (2004). Modern UV-VIS spectroscopy: a decade of fiber-optic CCD array spectrophotometers. *Am. Lab.,* **36**(15): 28-29.

Rajan RP and Ghosh A (2012). Angular amplification by a diffraction grating for chiro-optical measurements. *Appl. Optics,* **51**(27): 6480-6483.

Schmidt W (1995). Novel single-beam optical spectrophotometer for fast luminescence, absorption, and reflection measurements of turbid materials. *Opt. Eng.,* **34**(2): 589-595.

Vargas-Vasquez SM, Romero-Zeron LB and Macmillan B (2010). Characterization of Cr (II) and Cr (III) acetate aqueous solutions using UV-VIS spectrophotometry and 1H NMR. *Chem. Eng. Commun.,* **197**(4): 491-505.

Zakharova AM, Grinshtein IL and Kartsova LA (2013). Determination of carbohydrates and sweeteners in foods and biologically active additives by high-performance liquid chromatography. *J. Anal. Chem.,* **68**(12): 1081-1084.

Zonios G (2010). Noise and stray light characterization of a compact CCD spectrophotometer used in biomedical applications. *Appl. Optics,* **49**(2): 163-169.